

# The properties of the T8.5p dwarf Ross 458C

Ben Burningham<sup>1\*</sup>, S. K. Leggett<sup>2</sup>, D. Homeier<sup>3</sup>, D. Saumon<sup>4</sup>, P.W. Lucas<sup>1</sup>,  
D. J. Pinfield<sup>1</sup>, C. G. Tinney<sup>5</sup>, F. Allard<sup>6</sup>, M. S. Marley<sup>7</sup>, H.R.A. Jones<sup>1</sup>,  
D. N. Murray<sup>1</sup>, M. Ishii<sup>8</sup>, A. D. Jones<sup>9</sup>, J. Gomes<sup>1</sup>, Z. Zhang<sup>1</sup>

<sup>1</sup> Centre for Astrophysics Research, Science and Technology Research Institute, University of Hertfordshire, Hatfield AL10 9AB

<sup>2</sup> Gemini Observatory, 670 N. A'ohoku Place, Hilo, HI 96720, USA

<sup>3</sup> Los Alamos National Laboratory, P.O. Box 1663, MS F663, Los Alamos, NM 87545, USA

<sup>4</sup> Institut für Astrophysik, Georg-August-Universität, Friedrich-Hund-Platz 1, 37077 Göttingen, Germany

<sup>5</sup> School of Physics, University of New South Wales, 2052. Australia

<sup>6</sup> C.R.A.L. (UMR 5574 CNRS), Ecole Normale Supérieure, 69364 Lyon Cedex 07, France

<sup>7</sup> NASA Ames Research Center, Mail Stop 245-3, Moffett Field, CA 94035, USA

<sup>8</sup> Subaru Telescope, 650 North A'ohoku Place, Hilo, HI 96720, USA

<sup>9</sup> Universidad de Chile, Camino el Observatorio # 1515, Santiago, Chile, Casilla 36-D

2 June 2019

## ABSTRACT

We present near-infrared photometry and spectroscopy, and warm-*Spitzer* IRAC photometry of the young very cool T dwarf Ross 458C, which we have typed as T8.5p. By applying the fiducial age constraints ( $\leq 1$  Gyr) imposed by the properties of the active M dwarf Ross 458A, we have used these data to determine that Ross 458C has  $T_{\text{eff}} = 695 \pm 60$  K,  $\log g = 4.0 - 4.7$  and an inferred mass of 5–20  $M_{\text{Jup}}$ . We have compared fits of the near-infrared spectrum and IRAC photometry to the BT Settl and Saumon & Marley model grids, and have found that both sets provide best fits that are consistent with our derived properties, whilst the former provide a marginally closer match to the data for all scenarios explored here. The main difference between the model grids arises in the 4.5  $\mu\text{m}$  region, where the BT Settl models are able to better predict the flux through the IRAC filter, suggesting that non-equilibrium effects on the CO-CO<sub>2</sub> ratio are important for shaping the mid-infrared spectra of very cool T dwarfs. We have also revisited the issue of dust opacity in the spectra of Ross 458C that was raised by Burgasser et al (2010). We have found that the BT Settl models which also incorporate a condensate cloud model, provide a better match to the near-infrared spectrum of this target than the Saumon & Marley model with  $f_{\text{sed}} = 2$ , and we briefly discuss the influence of condensate clouds on T dwarf spectra.

**Key words:** surveys - stars: low-mass, brown dwarfs

## 1 INTRODUCTION

Precise determination of the fundamental properties (i.e. mass, age, metallicity and effective temperature,  $T_{\text{eff}}$ ) of isolated old brown dwarfs poses some serious challenges. These principally arise because (a) brown dwarfs cool over time, and (b) ages are one of the most difficult parameters to measure for field stars and brown dwarfs. Together this makes breaking the degeneracies between age, mass, luminosity and effective temperature for isolated brown dwarfs extremely difficult. An object with  $T_{\text{eff}} = 1000$  K, for example, might be relatively young and low-mass (e.g. 500 Myr and 20  $M_{\text{Jup}}$ ),

or it could equally be older and higher-mass (e.g. 10 Gyr and 60  $M_{\text{Jup}}$ ). Furthermore, determination of  $T_{\text{eff}}$  for such objects is itself problematic due to the fact that the radii of brown dwarfs must be estimated using evolutionary models (e.g. Baraffe et al. 2003; Saumon & Marley 2008) which to date have yet to be constrained by direct measurement of field brown dwarf radii<sup>1</sup>. The lack of age constraints for isolated brown dwarfs makes such estimates particularly uncertain. The influence of metallicity on the emergent spectra

<sup>1</sup> Although radii for a handful of brown dwarfs in cataclysmic variable (e.g. Littlefair et al. 2007) and young eclipsing systems (e.g. Stassun et al. 2006) have been measured these objects are not representative of the field population.

\* E-mail: B.Burningham@herts.ac.uk

from brown dwarfs further complicates matters, and so the calibration of model spectra using systems with well understood age and metallicity constraints is key to improving our understanding of sub-stellar atmospheres. For these reasons, much effort has been expended identifying and characterising systems for which dynamical masses may be measured (e.g. Scholz et al. 2003; Dupuy et al. 2009; King et al. 2010, and references therein) or age and metallicity fiducially constrained (e.g. Pinfield et al. 2006; Burningham et al. 2009; Day-Jones et al. 2008, 2010; Zhang et al. 2010).

Goldman et al. (2010) report the discovery of one such age and metallicity benchmark system, a candidate T8+ dwarf identified in the UKIRT Infrared Deep Sky Survey (UKIDSS; Lawrence et al. 2007) that has been shown to be a common proper motion companion to the M0.5+M7 binary system Ross 458AB. Using gyrochronology arguments and the age-activity relations of West et al. (2008), Goldman et al. (2010) constrain the age of Ross 458AB to less than 1Gyr. They also highlight its possible membership of the Hyades moving group, although conflicting radial velocity measurements by Hawley et al. (1997) and Nidever et al. (2002) leave this in doubt. However, given the spread in age and metallicity seen for members of the Hyades moving group, it is not immediately clear that such membership would permit any tighter constraints to be placed on the properties of the Ross 458 system than are possible otherwise. Burgasser et al. (2010) used the  $M_K$ /metallicity and  $V - K$ /metallicity relations of Johnson & Apps (2009) and Schlafman & Laughlin (2010) to estimate metallicities of  $[M/H] = +0.20 \pm 0.05$  and  $0.31 \pm 0.05$  for the Ross 458 system. The young ( $\leq 1$  Gyr) age of the system, though, means that it is not immediately clear that such relations can be applied with confidence. We return to this point at the end of Section 3.2.

The first estimate of Ross 458C's spectral type was made through deep methane imaging by Goldman et al. (2010). It was subsequently and independently identified as part of an ongoing large program to identify the coolest T dwarfs in the UKIDSS Large Area Survey (LAS) (e.g. Lodieu et al. 2007; Pinfield et al. 2008; Burningham et al. 2008, 2009, 2010a). As part of that program we have obtained near-infrared spectroscopy, as well as additional near-infrared and warm-*Spitzer* photometry which we use here to estimate the properties for this object.

Recently, Burgasser et al. (2010) has presented spectroscopy of Ross 458C deriving a spectral type of T8. They also compared their spectroscopy to a number of Saumon et al. (2006, 2007) model spectra to derive properties. They found that model spectra with significant condensate opacity provided a better match to their data than cloudless models. In Section 3.2 we compare our data to models from the Saumon & Marley grid, and also to the latest BT Settl model grid, which also includes a condensate cloud model (Allard et al. 2010).

## 2 NEW OBSERVATIONS OF ROSS 458C

### 2.1 Near-infrared photometry

Near-infrared follow-up photometry was obtained using the Wide Field CAMera (WFCAM; Casali et al. 2007) on

UKIRT on the night of 17<sup>th</sup> June 2009, and the data were processed using the WFCAM science pipeline by the Cambridge Astronomical Surveys Unit (CASU) (Irwin et al. 2004), and archived at the WFCAM Science Archive (WSA; Hambly et al. 2008). Observations consisted of a three point jitter pattern in the  $Y$  and  $J$  bands, and five point jitter patterns in the  $H$  and  $K$  bands repeated twice. All data were acquired with 2x2 microstepping and individual exposures of 10 seconds resulting in total integration times of 120 seconds in  $Y$  and  $J$  and 400 seconds in  $H$  and  $K$ . The WFCAM filters are on the Mauna Kea Observatories (MKO) photometric system (Tokunaga et al. 2002).

The resulting photometry is given in Table 1. It should be noted that the follow-up WFCAM data are generally in good agreement with the survey data, with the exception of the  $Y$  band, for which there is a  $9\sigma$  disagreement. The origin of this discrepancy is not clear.

### 2.2 Warm-*Spitzer* photometry

Data were obtained for Ross 458C on 13<sup>th</sup> March 2010, via the Cycle 6 GO program 60093. Individual frame times were 30 seconds repeated three times, with a 16-position spiral dither pattern, for a total integration time of 24 minutes in each of the [3.6] and [4.5] bands. The post-basic-calibrated-data (pbcd) mosaics generated by version 18.14.0 of the *Spitzer* pipeline were used to obtain aperture photometry. The photometry was derived using a 7'' aperture, and the aperture correction was taken from the IRAC handbook<sup>2</sup>. The error is estimated by the larger of either the variation with sky aperture, or the error implied by the uncertainty images. This error is small (Table 1) and is dominated by the 3% error that should be added in quadrature to the quoted random errors to account for systematic effects due to calibration uncertainties and pipeline dependencies.

### 2.3 Near-infrared spectroscopy

We used  $JH$  and  $HK$  grisms in the InfraRed Camera and Spectrograph (IRCS; Kobayashi et al. 2000) on the Subaru telescope on Mauna Kea to obtain a  $R \sim 100$   $JH$  and  $HK$  spectra for Ross 458C on 7<sup>th</sup> May 2009 and 31<sup>st</sup> December 2009 respectively. The observations were made up of a set of four 300s sub-exposures for the  $JH$  spectrum and six 240s sub-exposures (obtained in an ABBA jitter pattern to facilitate background subtraction), with a slit width of 0.6 arcsec delivering a resolution of  $R \sim 100$ . In addition we obtained a deep  $H$  band spectrum using the Near InfraRed Imager and Spectrometer (NIRI; Hodapp et al. 2003) on the Gemini North Telescope<sup>3</sup>. The NIRI observations were made up of twelve 300s sub-exposures observed in an ABBA jitter, with a 1 arcsecond slit delivering a resolution of  $R \sim 500$ .

The spectra were extracted using standard IRAF packages. The AB pairs were subtracted using generic IRAF tools, and median stacked. In the case of IRCS, the data were found to be sufficiently uniform in the spatial axis for flat-fielding to be neglected. We used a comparison argon arc

<sup>2</sup> <http://ssc.spitzer.caltech.edu/irac/dh/>

<sup>3</sup> under program GN-2009B-Q-62

$z'_{SDSS}$	$Y_{UKIDSS}$	$J_{UKIDSS}$	$H_{UKIDSS}$	$K_{UKIDSS}$		
$20.24 \pm 0.19$	$17.72 \pm 0.02$	$16.69 \pm 0.01$	$17.01 \pm 0.04$	$16.90 \pm 0.06$		
$Y_{WFCAM}$	$J_{WFCAM}$	$H_{WFCAM}$	$K_{WFCAM}$	[3.5]	[4.5]	
$17.54 \pm 0.02$	$16.71 \pm 0.01$	$17.07 \pm 0.03$	$16.96 \pm 0.03$	$15.28 \pm 0.01$	$13.77 \pm 0.01$	
$z'_{SDSS} - J_{WFCAM}$	$Y_{WFCAM} - J_{WFCAM}$	$J_{WFCAM} - H_{WFCAM}$	$H_{WFCAM} - K_{WFCAM}$	$H_{WFCAM} - [4.5]$	[3.5]-[4.5]	
$3.53 \pm 0.19$	$0.83 \pm 0.02$	$-0.36 \pm 0.03$	$0.11 \pm 0.04$	$3.30 \pm 0.03$	$1.15 \pm 0.02$	

**Table 1.** Summary of photometry for Ross 458C. The subscripts on the column headings indicated the source of the data, where: “UKIDSS” indicates UKIDSS survey data; “SDSS” indicates; “WFCAM” indicates WFCAM follow-up photometry.

frame to obtain the dispersion solution, which was then applied to the pixel coordinates in the dispersion direction on the images. The resulting wavelength-calibrated subtracted pairs had a low-level of residual sky emission removed by fitting and subtracting this emission with a set of polynomial functions fit to each pixel row perpendicular to the dispersion direction, and considering pixel data on either side of the target spectrum only. The spectra were then extracted using a linear aperture, and cosmic rays and bad pixels removed using a sigma-clipping algorithm.

Telluric correction was achieved by dividing each extracted target spectrum by that of an F5 star, observed just before or after the target and at a similar airmass. Prior to division, hydrogen lines were removed from the standard star spectrum by interpolating the stellar continuum. Relative flux calibration was then achieved by multiplying through by a blackbody spectrum of the appropriate  $T_{\text{eff}}$ .

The IRCS  $JH$  and  $HK$  spectra were joined by scaling them to match at the  $H$  band peak (at  $1.58\mu\text{m}$ ). The higher signal-to-noise NIRI  $H$  band spectrum was then used to replace the  $H$  band region of the IRCS spectra, again by scaling it to match the IRCS spectrum at  $1.58\mu\text{m}$ . We note here that the NIRI spectrum closely traced the shape of the noisier IRCS spectra in this region.

## 2.4 Spectral type

We have assigned a spectral type for Ross 458C following the scheme laid out by Burgasser et al. (2006) and extended by Burningham et al. (2008). Figure 1 shows our combined IRCS+NIRI  $JHK$  spectrum for Ross 458C along with spectra for the T8 and T9 templates 2MASS J04151954-093506.6 and ULAS J133553.45+113005.2. Whilst the spectrum of Ross 458C lies roughly between the T8 and T9 spectra in the  $J$  band, it appears to be earlier in type in the  $H_2O-H$  region, and there is considerable excess flux in the  $K$  band.

The spectral flux ratios for Ross 458C are given in Table 2. Their values reflect the qualitative comparison with the spectral templates described above. The mismatch in inferred spectral type between the three indices that are not degenerate ( $W_J$ ,  $H_2O-H$ ,  $CH_4-K$ ) makes assigning a spectral type for this object problematic. The remaining index values are all consistent with a type later than T7, in disagreement with the  $H_2O-H$  and  $CH_4-K$  indices but in agreement with the  $W_J$  index. We thus allow the  $W_J$  index to dominate the classification, and assign a type of T8.5p ( $\pm 0.5$ ), reflecting the close agreement between the T8 and

T9 spectra in the  $J$  band, and highlighting the peculiarity of the spectrum elsewhere.

This spectral type is consistent with that estimated for Ross 458C from methane imaging (T8.9, Goldman et al. 2010), and also that found by Burgasser et al. (2010). However, it disagrees with the type of T7 found by Scholz (2010) using a combination of  $JHK$  colour-colour plots and absolute magnitude arguments. This is driven by the weight Scholz (2010) places on the estimates from  $J-H/J-K$  colour-colour plots, which suggest an early type of T4.0–T6.5. Since the colours of Ross 458C are fairly typical of other T8+ dwarfs discovered to date, it would appear that such plots have little utility in spectral typing the latest type T dwarfs.

The disagreement between the  $W_J$  index and the  $H_2O-H$  index that is seen in Ross 458C is broadly consistent with the unusual spectral morphology referred to as “ $H_2O-H$ -early” peculiarity by Burningham et al. (2010b). In addition to Ross 458C, two other  $\geq T7$  dwarfs have been identified that display this peculiarity: the T8p dwarf ULAS J101721.40+011817.9 (Burningham et al. 2008) and the T7p dwarf Gl 229B (Nakajima et al. 1995; Burgasser et al. 2006). Several earlier type T dwarfs have also been identified with this peculiarity and are described in Burningham et al. (2010b).

It is interesting to note that both Gl 229B and ULAS J1017+0118 have inferred ages similar to that for Ross 458C, the former implied by the activity of its M0.5 primary star (e.g. West et al. 2008) and the latter by comparison of near- and mid-infrared photometry to model predictions (Leggett et al. 2010). However, interpretation of the  $H_2O-H$  early peculiarity as being directly connected to the relative youth of these systems is probably premature, particularly in light of the recent observation that amongst the earlier-type objects that display this morphology described in Burningham et al. (2010b), one has emerged to exhibit halo kinematics (Murray et al. in prep).

## 3 THE PROPERTIES OF ROSS 458C

### 3.1 Luminosity and effective temperature

We estimate the bolometric flux ( $F_{\text{bol}}$ ) of Ross 458C following the method outlined in Burningham et al. (2009), by combining our  $JHK$  spectra (flux calibrated by our WFCAM follow-up photometry) with model spectra (to allow us to estimate the flux contributions from regions outside our near-infrared spectral coverage). We have scaled the

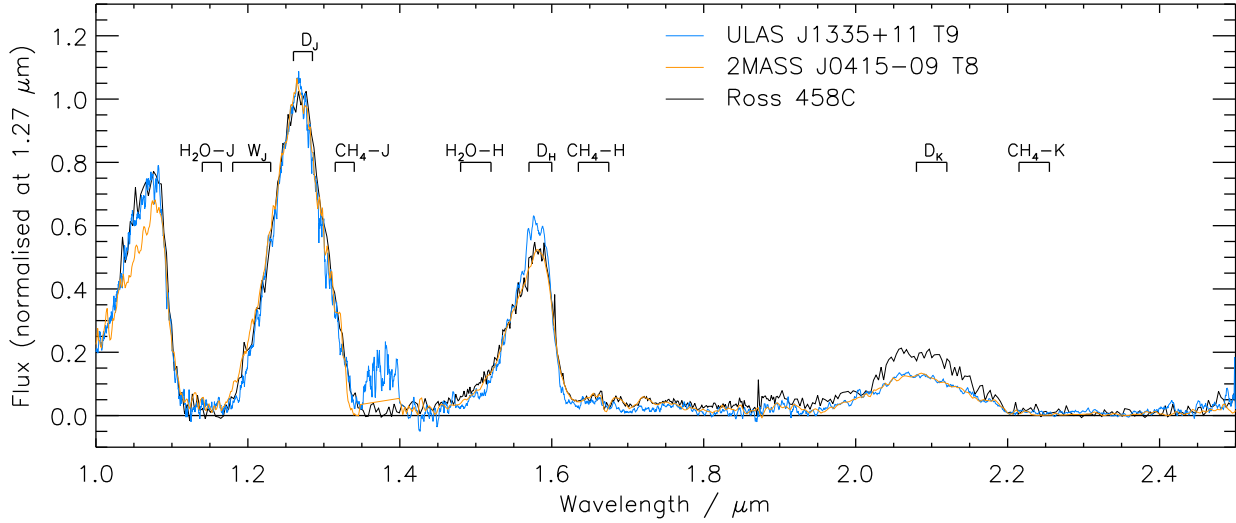


**Figure 1.** The IRCS+NIRI *JHK* spectrum for Ross 458C plotted with T8 and T9 spectral standards 2MASS J04151954–093506.6 and ULAS JJ133553.45+113005.2. Overlaid are the spectral ranges for the numerators (indicated by the index for which they apply) and denominators (D; subscript indicates the index set) of the spectral typing indices used in Table 1 and outlined in Burgasser et al. (2006) and Burningham et al. (2008).

Index	Ratio	Value	Type
H <sub>2</sub> O-J	$\frac{\int_{1.14}^{1.165} f(\lambda)d\lambda}{\int_{1.26}^{1.285} f(\lambda)d\lambda}$	$0.007 \pm 0.004$	$\geq$ T8
CH <sub>4</sub> -J	$\frac{\int_{1.315}^{1.34} f(\lambda)d\lambda}{\int_{1.26}^{1.285} f(\lambda)d\lambda}$	$0.20 \pm 0.01$	$\geq$ T8
<i>W<sub>J</sub></i>	$\frac{\int_{1.18}^{1.23} f(\lambda)d\lambda}{2 \int_{1.26}^{1.285} f(\lambda)d\lambda}$	$0.27 \pm 0.01$	T8/9
H <sub>2</sub> O-H	$\frac{\int_{1.48}^{1.52} f(\lambda)d\lambda}{\int_{1.56}^{1.60} f(\lambda)d\lambda}$	$0.22 \pm 0.01$	T7
CH <sub>4</sub> -H	$\frac{\int_{1.635}^{1.675} f(\lambda)d\lambda}{\int_{1.56}^{1.60} f(\lambda)d\lambda}$	$0.11 \pm 0.01$	$\geq$ T8
NH <sub>3</sub> -H	$\frac{\int_{1.53}^{1.56} f(\lambda)d\lambda}{\int_{1.57}^{1.60} f(\lambda)d\lambda}$	$0.71 \pm 0.01$	...
CH <sub>4</sub> -K	$\frac{\int_{2.215}^{2.255} f(\lambda)d\lambda}{\int_{2.08}^{2.12} f(\lambda)d\lambda}$	$0.20 \pm 0.01$	T5

**Table 2.** The spectral flux ratios for Ross 458C. The locations of the numerators and denominators are indicated on Figure 1. The NH<sub>3</sub> index is not used for assigning a type (see Burningham et al. 2008, and Burningham et al 2010 for a discussion of this), but is included for completeness and to permit future comparison with other late T dwarfs.

$\lambda < 1.05\mu\text{m}$  region of the models to match the flux level in our *JHK* spectrum, whilst we have used the warm-*Spitzer* channel 1 and 2 photometry to scale the 2.5–4.0

$\mu\text{m}$  and  $\lambda > 4.0\mu\text{m}$  regions respectively. To provide some indication of the systematic effects of our choice of atmospheric models we have estimated the bolometric flux using both BT Settl models (Allard et al. 2008) and those of Saumon et al. (2006, 2007).

We initially selected BT Settl model spectra covering the  $T_{\text{eff}} = 500\text{--}750\text{K}$  range,  $\log g = 4.0\text{--}5.0$  and  $[M/H] = 0.0$  and  $+0.3$ . This range of parameters was selected to ensure that we include all likely possibilities for such a young and late-type T dwarf, and allowing for the potentially high metallicity suggested by Burgasser et al. (2010). We then took the median as our value for  $F_{\text{bol}}$ , and the scatter in values as an estimate of the systematic uncertainty associated with our use of theoretical extensions scaled to photometry, amounting to approximately 11%. The uncertainties in the photometry used to scale the model spectra contribute approximately 4% to the flux error budget. We thus estimate for Ross 458C that  $F_{\text{bol}} = 6.40 \pm 0.80 \times 10^{-16} \text{Wm}^{-2}$ , of which approximately 60% is emitted longward of  $2.4\mu\text{m}$ . Using the well determined distance to the primary star, and incorporating the uncertainty therein, we estimate the total luminosity of Ross 458C to be  $2.59 \pm 0.34 \times 10^{-6} L_{\odot}$ .

We used the Saumon et al. (2006, 2007) models to fill in the missing spectral regions in an identical manner to that described above for the BT Settl model grid. We selected cloudless models across the same temperature, gravity and metallicity range as used for the BT Settl bolometric correction, and for simplicity at this stage we have considered only a single eddy diffusion coefficient (which parameterises non-equilibrium effects due to turbulent mixing - see below) of  $\log K_{zz} = 4$ . This value has been selected as simply a typical one for late T dwarfs, and does represent a firm estimate for the value of this parameter for Ross 458C, and selecting a different value does not affect our flux estimate, since we scale our model spectra by the observed photometry. In Section 3.2 we find the best fitting value of  $\log K_{zz}$ .

We find that this choice of models for our bolometric correction suggests a value of  $F_{bol} = 6.06 \pm 0.42 \times 10^{-16} \text{ Wm}^{-2}$ , with a 7% contribution to the uncertainty arising from the scatter in the model extensions. We find that essentially the same contribution to the correction arises from the region longward of  $2.4\mu\text{m}$ . Our estimate for the total luminosity of Ross 458C using the Saumon & Marley model set is thus  $2.45 \pm 0.20 \times 10^{-6} L_{\odot}$ , which is consistent with the estimate derived using the BT Settl model grid. Both estimates for  $L_{bol}$  are substantially brighter than has been found for the similarly typed late-T dwarf Wolf 940B (Burningham et al. 2009; Leggett et al. 2010) for which  $9.79 \times 10^{-7} L_{\odot}$  has been estimated (Leggett et al. 2010).

To determine  $T_{\text{eff}}$  for Ross 458C we have used the constraints placed on its age by Goldman et al. (2010) to estimate a likely range of radii. As with the bolometric correction, we have used two sets of evolutionary models to provide some indication of the systematic effects involved in this process. Using predictions from the COND (Baraffe et al. 2003) evolutionary models, for the  $0.1 \leq \text{age} \leq 1\text{Gyr}$  range, we find that our derived luminosity estimates are consistent with a radius in the  $0.101\text{--}0.120 R_{\odot}$  interval (and  $\log g = 4.7$  and  $4.0$  respectively). This results in an inferred  $T_{\text{eff}}$  range of  $730 \pm 25\text{K}$  to  $670 \pm 20\text{K}$  for our BT Settl based bolometric correction, and a range of  $720 \pm 15$  to  $660 \pm 15$  for our Saumon & Marley corrected luminosity.

Using the evolutionary tracks of Saumon & Marley (2008) suggests a slightly larger radius than the COND models, with a radius in the range  $0.103\text{--}0.124 R_{\odot}$  (and  $\log g = 4.7$  and  $4.0$  respectively), resulting in lower inferred values for  $T_{\text{eff}}$ , with ranges of  $720 \pm 25\text{K}$  to  $660 \pm 20\text{K}$  and  $710 \pm 15\text{K}$  to  $650 \pm 15\text{K}$  for our BT Settl and Saumon & Marley corrected luminosities respectively.

Although the BT Settl bolometric correction suggests a marginally higher  $T_{\text{eff}}$  range, the two estimates are consistent and we adopt  $T_{\text{eff}} = 695 \pm 60\text{K}$  as our final estimate, with  $\log g = 4.0\text{--}4.7$ . For our age constraint of  $0.1\text{--}1\text{Gyr}$  this corresponds to a mass range of roughly  $5\text{--}20 M_J$  according to both sets of evolutionary models.

### 3.2 Model comparison

In Figure 2, we have compared model spectra for a range of parameters that straddle our  $T_{\text{eff}}$  and gravity estimates for Ross 458C with the observed spectrum and the mean fluxes inferred for the warm-*Spitzer* channel 1 and 2 photometry. On the whole the BT Settl models appear to provide the best fits in the near-infrared although, as has been seen before (Burningham et al. 2009), their  $K$  band flux is substantially underestimated. Of note also is the difference between the two model sets in the  $1.57\text{--}1.60\mu\text{m}$  region, where missing methane opacities are thought to be a significant factor in the generally poor fit of model spectra to data in this region. Both model sets base their methane opacities on the same incomplete line lists, however the BT Settl model grid use a statistical estimate of the contributions from hot vibrational bands in the  $H$  and  $K$  bands, based on the results of Borysov et al. (2003), and this may account for the differences seen in the  $H$  band absorption features.

The most notable differences between the two model sets, however, lie in the  $3.5\text{--}5\mu\text{m}$  region, where the BT Settl

models are able to match both the [3.5] and [4.5] fluxes well. The Saumon & Marley models, on the other hand, tend to somewhat underestimate the flux in the former and overestimate the flux in the latter. Both model sets predict similar absorption strengths for the CO fundamental band at  $4.55\mu\text{m}$ , but a significant difference in the integrated [4.5] fluxes arises from a much stronger CO<sub>2</sub> band centered at  $4.3\mu\text{m}$  in the BT Settl models than is seen in the Saumon & Marley models. Both sets of models use similar CO<sub>2</sub> opacities and the same CNO abundances, but the BT Settl consider chemical non-equilibrium effects on the CO<sub>2</sub> to CO mixing ratio and thus could be expected have higher carbon dioxide abundances in the upper atmosphere.

To examine this possibility in more detail we have recalculated the BT Settl model spectrum for the  $T_{\text{eff}} = 700\text{K}$ ,  $\log g = 4.5$ , Solar metallicity case under several different assumptions about CO and CO<sub>2</sub> chemistry. The left side of Figure 3 compares the  $3.5\text{--}5.5\mu\text{m}$  region for the BT Settl models under the following cases: CE - carbon species in full chemical equilibrium; R0 - equal reduction rate for CO<sub>2</sub> and CO; R1 - includes the reaction of CO with OH for the conversion between CO and CO<sub>2</sub>, as used by Visscher et al. (2010) for the Jovian atmosphere; R2 - this is the standard BT Settl treatment and is as for R1 but also includes the reaction of CO with H<sub>2</sub>O. The R0 case is roughly equivalent to the treatment in the Saumon & Marley models, and the right side of Figure 3 shows that this case compares much more closely than the two CO<sub>2</sub> non-equilibrium cases. This supports the assertion that the principal cause of the difference between the two model groups in this region is the non-equilibrium treatment for CO<sub>2</sub> chemistry used by the BT Settl models.

We note that the default BT Settl (R2) case produces a between five and six times higher CO<sub>2</sub> abundance than with the single reaction for converting CO to CO<sub>2</sub>, and 30–40 times higher CO<sub>2</sub> abundance than in the case where both CO and CO<sub>2</sub> are quenched at the same level (as in the Saumon & Marley models). The increased abundance of CO<sub>2</sub> does not impact the CO-CH<sub>4</sub> chemistry significantly since CO remains over 20 times more abundant than CO<sub>2</sub> even in the default BT Settl (R2) model, and CH<sub>4</sub> number density is similarly unaffected by any of the chemistry models since it always remains two orders of magnitude more abundant than CO.

It is clear then that it is appropriate to attribute the difference between the models in the  $4.3\mu\text{m}$  region to the non-equilibrium treatment of CO<sub>2</sub> in the BT Settl models, and that the strength of the CO<sub>2</sub> absorption is also strongly dependent on which reaction paths are considered. The better fit of the BT Settl models to the observed warm-*Spitzer* photometry suggests that such effects are important for determining the emergent spectra of very cool T dwarfs. The non-equilibrium treatment for CO<sub>2</sub> chemistry is further supported by the recent identification of strong  $4.3\mu\text{m}$  CO<sub>2</sub> absorption in *AKARI* / IRC spectroscopy of the T8 dwarf 2MASS J04151954-0935066 (Yamamura et al. 2010), although it is not yet established if both reaction pathways considered in the BT Settl models are at work in such environments.

To quantitatively assess the best fitting model we have employed the goodness-of-fit statistic,  $G$ , of Cushing et al. (2008) which is defined for a given model,  $k$  as

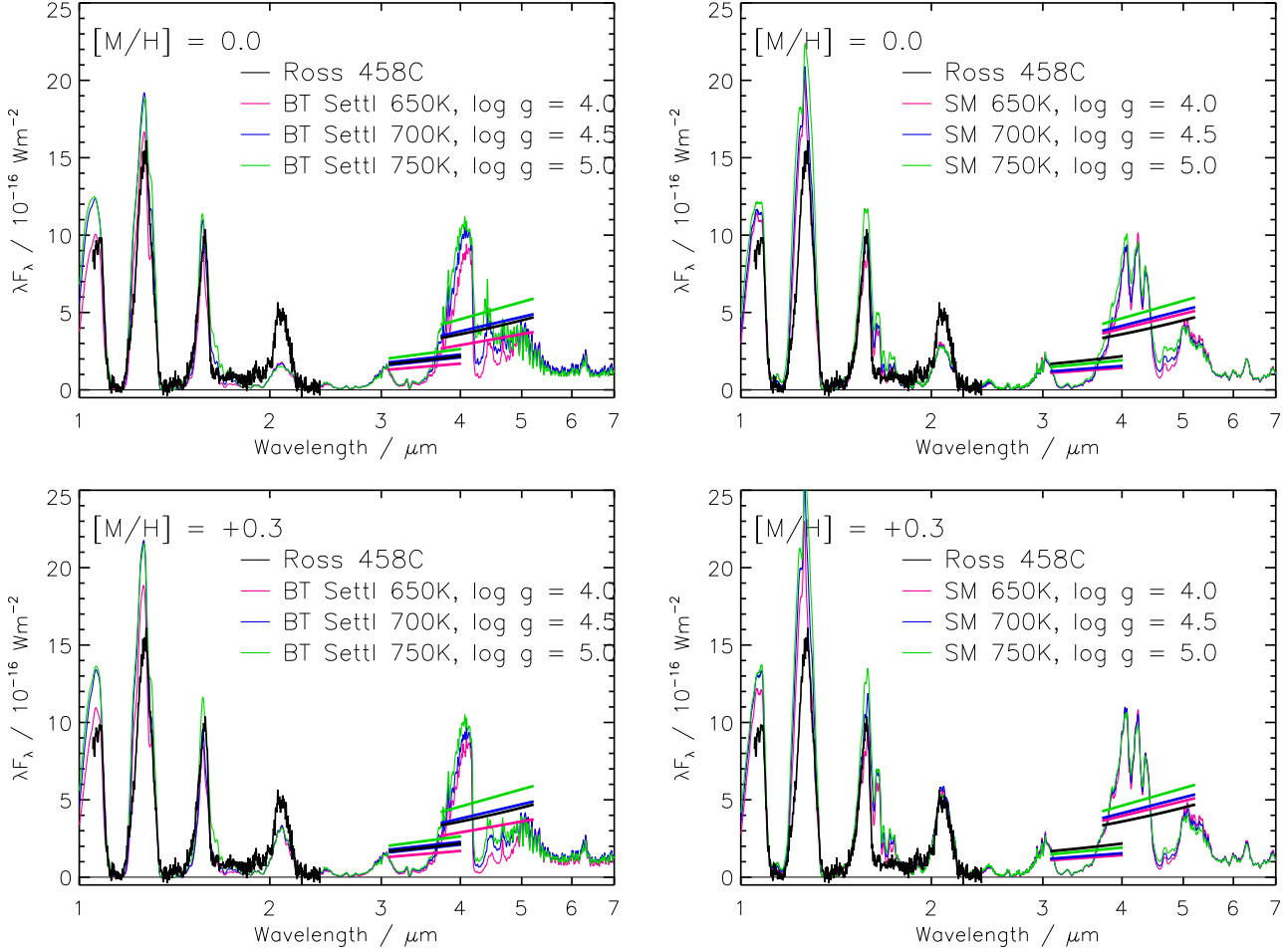


**Figure 2.** The *JHK* spectrum of Ross 458C and mean fluxes inferred from the warm-*Spitzer* photometry compared to model spectra that straddle the properties estimated in Section 3.1. In the case of the Saumon & Marley models, we found that the model grid for which  $\log K_{zz} = 6$ , provided the best match to the data, and this is what has been plotted here. The straight coloured lines indicate the mean fluxes of model spectra in the *Spitzer* photometric bands and plotted to allow comparison with the mean flux from the target (straight black lines).

$$G_k = \sum_{i=1}^n w_i \left( \frac{f_i - C_k F_{k,i}}{\sigma_i} \right)^2 \quad (1)$$

where  $w$  is the weight to be assigned to wavelength interval,  $i$ ,  $f$  is the observed flux with uncertainty  $\sigma$ ,  $F$  is the model flux and  $C$  is a scaling factor equal to  $R^2/D^2$  for a source of radius  $R$  at distance  $D$ . We take the value of the weight  $w$  as the width in wavelength space of each point on the spectrum. In all cases we convolved the model spectra with the instrumental profile of the observed spectrum of Ross 458C such that the resolutions are equivalent. In applying this statistic we have treated the total flux captured through each warm-*Spitzer* filter as a single point, weighted by the width of the filter. Uncertainties in the value of  $G$  have been calculated by performing 10000 Monte Carlo simulations for each case, randomly offsetting the target spectrum according to the measured uncertainties.

In Figure 4 we have plotted the values for  $G$  for various  $T_{\text{eff}}$  and  $\log g$  for both sets of models. We have computed  $C$  using the known parallax of Ross 458AB and radii consistent with the values of  $\log g$  as implied by both sets of

evolutionary models. We have also calculated  $G$  for the case where the scaling factor  $C$  is unconstrained by parallax and evolutionary arguments to determine the  $T_{\text{eff}}$  estimate that would be found from pure spectral fitting in the case of the two sets of models, and the results are plotted in Figure 5. We have summarised the best fitting models for each case in Table 3.

The best fitting model spectra in both the free scaling fits and the constrained  $R/D$  fits suggest properties that are consistent with those estimated from our empirically determined luminosity for Ross 458C. That the best fits are all provided by the Solar metallicity BT Settl models appears inconsistent with the  $[M/H] = +0.2$ – $+0.3$  estimates for the system from Burgasser et al. (2010). However, the  $M_K$ /metallicity and  $V - K$ /metallicity relations of Johnson & Apps (2009) and Schlaufman & Laughlin (2010) that were applied in that work are based on calibration from a relatively small number of M dwarfs, and Ross 458A lies at the early spectral type extreme of the sample. Additionally, the calibration samples are likely dominated by systems with ages typically larger than 3 Gyr. Such systems show little

Case	BT Settl best fit			SM best fit		
	$T_{\text{eff}}$	$\log g$	$G$	$T_{\text{eff}}$	$\log g$	$G$
[M/H] = 0.0, fixed $C_k$	700 K	4.5	$18.7 \pm 0.8$	650 K	4.0	$58.5 \pm 6.8$
[M/H] = +0.3, fixed $C_k$	750 K	5.0	$30.5 \pm 2.7$	650 K	4.0	$38.6 \pm 4.3$
[M/H] = 0.0, free $C_k$	750 K	5.0	$16.6 \pm 0.7$	750 K	4.0	$33.1 \pm 2.7$
[M/H] = +0.3, free $C_k$	700 K	5.0	$19.8 \pm 1.2$	700 K	4.0	$27.7 \pm 1.7$

**Table 3.** Summary of the best fit model spectra and their associated  $G$  values.

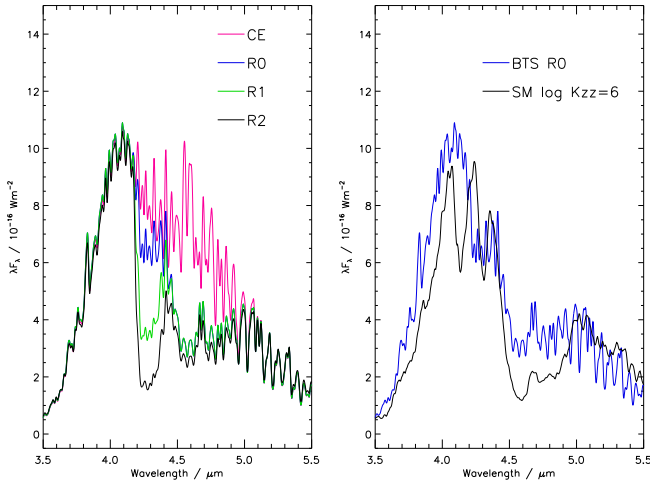


**Figure 3.** Left: A comparison of different treatments of carbon chemistry in the BT Settl model grid for a Solar metallicity,  $T_{\text{eff}} = 700\text{K}$ ,  $\log g = 4.5$  atmosphere where: CE = carbon species in full chemical equilibrium; R0 = equal reduction rate for  $\text{CO}_2$  and CO; R1 = includes the reaction of CO with OH for the conversion between CO and  $\text{CO}_2$ ; R2 = as for R1 but also includes the reaction of CO with  $\text{H}_2\text{O}$ . Right: A comparison of the R0 case with the Saumon & Marley model for the same atmospheric parameters and  $\log K_{zz} = 6$ .

evolution in the  $(V - K_s) - M_K$  plane with age, and thus any spread about the main sequence may be attributed to metallicity, however the same can not be said for dwarfs with the young age of Ross 458. Burgasser et al. (2010) also noted that the young age of Ross 458 may introduce a bias to higher metallicity, and Morales et al. (2008) found systematically higher values of  $[\text{Fe}/\text{H}]$  for active stars when using the Bonfils et al. (2005) relations.

### 3.3 Dust in the atmosphere of Ross 458C

In Figure 6 we have plotted the goodness-of-fit statistic,  $G$ , minimised for the case of a free scale factor,  $C$ , for Saumon & Marley models in which condensate clouds are present in the photosphere and for BT Settl models. The Saumon & Marley atmospheres use the Ackerman & Marley (2001) cloud model, which parameterises the efficiency of sedimentation of condensate particles through an efficiency factor  $f_{\text{sed}}$ . Larger values represent faster particle growth and larger mean grain sizes. Larger dust grains rain out of the atmosphere giving rise to optically thin clouds. Smaller values of  $f_{\text{sed}}$  thus correspond to thicker clouds.

Since no Saumon & Marley models with dust clouds

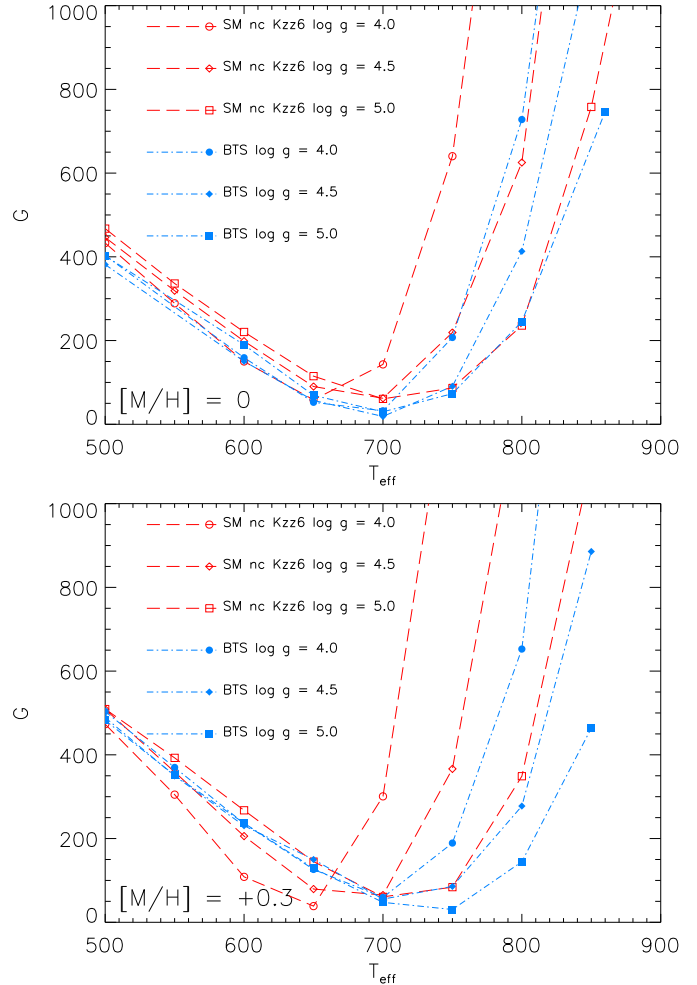


**Figure 4.** The goodness-of-fit statistic,  $G$ , plotted for various model spectra with the value of the scaling factor  $C$  fixed by evolutionary considerations and the measured parallax to Ross 458AB. For simplicity we only plot the best fitting case of  $\log K_{zz} = 6$  for the Saumon & Marley model grid.

are currently available for  $\log K_{zz} = 6$ , we have only fitted the near infrared spectrum since a lower value of  $K_{zz}$  will result in a poor fit at longer wavelengths which would tend to dominate the statistic. We found that the best fit for the Saumon & Marley models was for a dust sedimentation efficiency parameter  $f_{\text{sed}} = 2$ , Solar metallicity,  $T_{\text{eff}} = 600\text{K}$  and  $\log g = 4.0$  ( $G = 28.03 \pm 0.3$ ). These properties are consistent with what was found by Burgasser et al. (2010), who found that Saumon & Marley models which included condensate opacity were able to provide a better fit to their

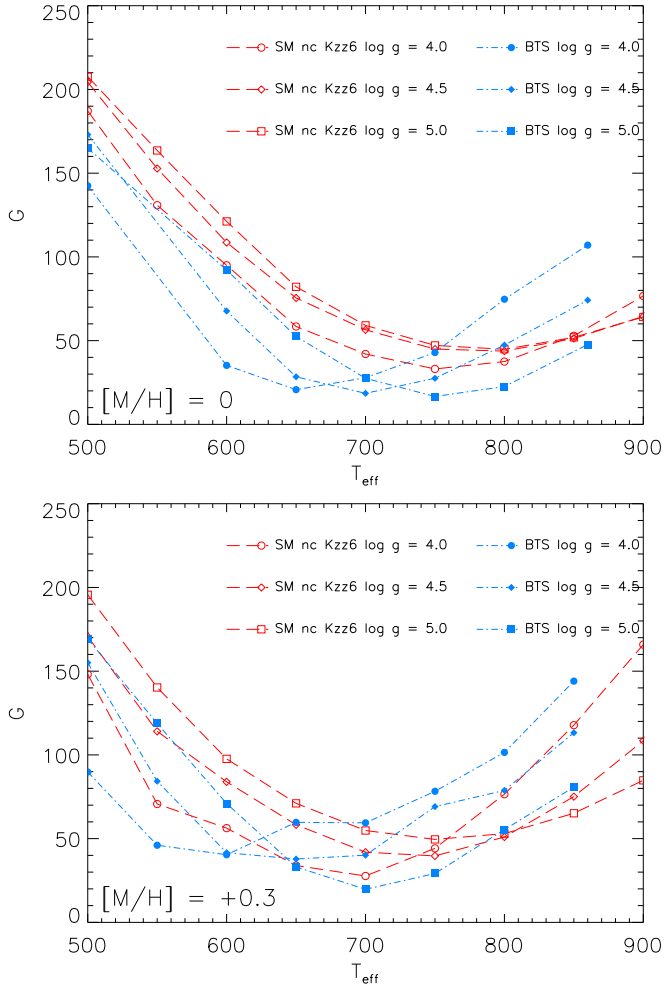


**Figure 5.** The goodness-of-fit statistic,  $G$ , plotted for various model spectra with the value of the scaling factor  $C$  evaluated such that  $G$  is minimised in each case (see Cushing et al. 2008). For simplicity we only plot the best fitting case of  $\log K_{zz} = 6$  for the Saumon & Marley model grid.

near infrared spectra than those without, leading them to conclude that condensate clouds are an important opacity source in very cool young T dwarf atmospheres. Whilst most of the cloud lies beneath the photosphere in this model, upper layers of cloud contribute to the near-infrared opacity, with an optical depth of  $\sim 0.8$  in the  $J$  band peak, such that the cloud is thick enough to define the photosphere in this region.

We have found that the BT Settl model with  $[M/H] = +0.3$ ,  $T_{\text{eff}} = 750\text{K}$  and  $\log g = 4.0$  provides a significantly better fit ( $G = 22.05 \pm 0.3$ ) than the dusty Saumon & Marley models in the restricted near-infrared fits examined in this Section. In the BT Settl models the main part of the cloud deck also lies well below the photosphere, but the upper cloud layers appear to have a smaller impact than in the case of the Saumon & Marley models. This small amount of cloud opacity may account for the better match of the BT Settl models in the  $J$  band peak compared to the cloud-free Saumon & Marley models (see Figure 2). We can thus conclude that whilst condensates contribute some near-infrared opacity at the low  $T_{\text{eff}}$  of cool T dwarfs, the use of mod-

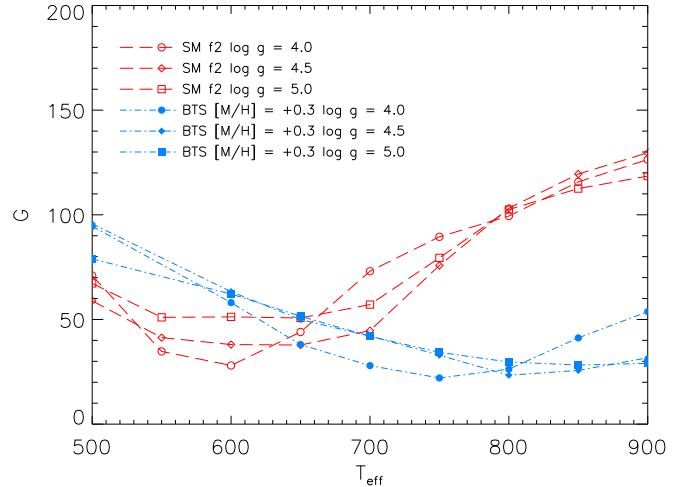


**Figure 6.** The goodness-of-fit statistic,  $G$ , plotted for various models, considering just the near-infrared portion of the spectra with the value of the scaling factor  $C$  evaluated such that  $G$  is minimised in each case (see Cushing et al. 2008).

els with clouds thinner in vertical extent than the  $f_{\text{sed}} = 2$  case is preferred. However, it should be noted that the difference in the dust opacity between the two models appears to be relatively modest. Whilst  $f_{\text{sed}} = 2$  corresponds to very dusty atmospheres at the  $T_{\text{eff}}$  of L dwarfs, it results in a roughly similar dust signature to the BT Settl models at  $T_{\text{eff}} = 700\text{K}$ .

We note, also, that the best fitting BT Settl models are somewhat warmer than is found when the IRAC photometry is included in the fit. This is likely due to the increased importance of the  $K$  band flux in the fit, which is consistently underestimated by the cool BT Settl models.

#### 4 COMPARISON TO THE WIDER LOW-TEMPERATURE SAMPLE

To place Ross 458C in context with the wider sample of very cool T dwarfs we have reproduced the  $H - K/H - [4.5]$  colour-colour plot of Leggett et al. (2010) in Figure 7. Although the behaviour of the  $H - [4.5]$  colour is likely poorly understood (see Section 3.2) and the models are known to produce  $H - K$  colours that are too blue, such a plot can still provide useful insights to the relative properties of the cool dwarf sample. The young age of Ross 458C and its location on this colour-colour plot would appear to support the assertion that the low-temperature T dwarfs identified in UKIDSS to date are dominated by young, low-mass objects (Leggett et al. 2010). This is interesting in the context of the dearth of late T dwarfs found in the Solar neighbourhood compared to what would be expected given the mass function seen in young cluster and associations (Burningham et al. 2010b), although it is not yet clear if this is due to some effect of the birthrate for brown dwarfs, an as yet unidentified selection effect or some problem with the evolutionary models.



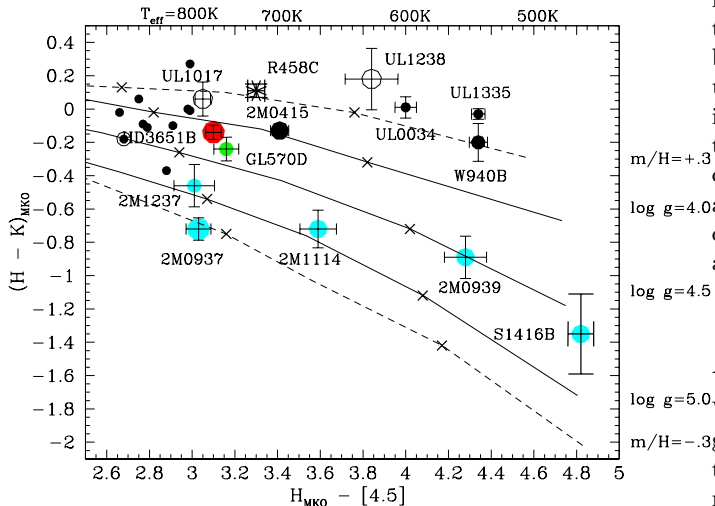


**Figure 7.** Near- to mid-infrared colours of cool T dwarfs compared to those of the Saumon & Marley model colours, after Figure 10 of Leggett et al. (2010).

## 5 SUMMARY

We have presented near-infrared spectroscopy, photometry and warm-*Spitzer* IRAC photometry of the very cool brown dwarf Ross 458C. We assign it the spectral type T8.5p, where the ‘p’ indicates the peculiarity due to an enhanced *K* band flux, presumably reflecting the low-gravity associated with such a young object. We have used both BT Settl and Saumon & Marley model grids to estimate the flux in regions not covered by our near-infrared spectrum and IRAC photometry, and by using age constraints placed on Ross 458AB by Goldman et al. (2010) we use the bolometric luminosity to estimate that  $T_{\text{eff}} = 695 \pm 60\text{K}$  and  $\log g = 4.0 - 4.7$ .

We have also fitted various model spectra to the data and have found that the Solar metallicity BT Settl model grid provide the best match to the data for our derived parameter set, although both model sets provide similar estimates for  $T_{\text{eff}}$  and gravity when used to fit for the parameters. The fitted estimates are also consistent with our determination from the bolometric flux.

We note, however, that these similar parameter estimates are despite significant differences in the predicted spectrum in the 4–5 $\mu\text{m}$  region due to differences in approach to CO–CO<sub>2</sub> chemistry. The BT Settl spectra best reproduce the IRAC photometry, suggesting that chemical non-equilibrium effects are important in setting the CO–CO<sub>2</sub> ratio, although spectroscopy would be required to confirm this assertion. The FLITECAM instrument (McLean et al. 2006) on board the Stratospheric Observatory for Infrared Astronomy (SOFIA; Becklin 2005) may provide the capability to distinguish the model sets for bright objects such as Ross 458C. For fainter objects, this spectral region will be restricted to photometric data until the launch of the James Webb Space Telescope.

We have also examined the suggestion by Burgasser et al. (2010) that condensate clouds are an important source of opacity in the emergent spectrum of Ross 458C. We find that the BT Settl models provide a better fit to the near infrared spectrum than the dusty

models favoured by the Burgasser et al. (2010) fits. Although in both sets of models the main cloud deck lies well below the photosphere, in the Saumon & Marley models the upper layers still effectively define the photosphere in near infrared spectral regions such as the *J* band peak, whilst in the BT Settl case their influence is much smaller. We thus conclude that condensate opacity does indeed appear to affect the near-infrared spectra of cool T dwarfs, although clouds with less vertical extent than is seen for the  $f_{\text{sed}} = 2$  are preferred.

## ACKNOWLEDGEMENTS

We thank our anonymous referee for comments that have greatly improved the quality of the manuscript. The authors wish to recognise and acknowledge the very significant cultural role and reverence that the summit of Mauna Kea has always had within the indigenous Hawaiian community. We are most fortunate to have the opportunity to conduct observations from this mountain. SKL is supported by the Gemini Observatory, which is operated by AURA, on behalf of the international Gemini partnership of Argentina, Australia, Brazil, Canada, Chile, the United Kingdom, and the United States of America. CGT is supported by ARC grant DP0774000. This research has made use of the SIMBAD database, operated at CDS, Strasbourg, France, and has benefited from the SpeX Prism Spectral Libraries, maintained by Adam Burgasser at <http://www.browndwarfs.org/spexprism>.

## REFERENCES

- Ackerman A. S., Marley M. S., 2001, *ApJ*, 556, 872  
 Allard F., Homeier D., Freytag B., 2010, *ArXiv e-prints*  
 Allard F., Homeier D., Freytag B., Guillot T., Chabrier G., Ludwig H., Allard N., Ferguson J., Barman T., Hauschildt P., 2008, *A&A*, in prep.  
 Baraffe I., Chabrier G., Barman T. S., Allard F., Hauschildt P. H., 2003, *A&A*, 402, 701  
 Becklin E. E., 2005, *Advances in Space Research*, 36, 1087  
 Bonfils X., Delfosse X., Udry S., Santos N. C., Forveille T., Ségransan D., 2005, *A&A*, 442, 635  
 Borysow A., Champion J. P., Jørgensen U. G., Wenger C., 2003, in *ASP Conference Series*, Vol. 288, *Stellar Atmosphere Modeling*, Hubeny I., Mihalas D., Werner K., eds., The Astronomical Society of the Pacific, San Francisco, pp. 352–356  
 Burgasser A. J., Geballe T. R., Leggett S. K., Kirkpatrick J. D., Golimowski D. A., 2006, *ApJ*, 637, 1067  
 Burgasser A. J., Simcoe R. A., Bochanski J. J., Saumon D., Mamajek E. E., Cushing M. C., Marley M. S., McMurtry C., Pipher J. L., Forrest W. J., 2010, *ArXiv e-prints*  
 Burningham B., Leggett S. K., Lucas P. W., Pinfield D. J., Smart R. L., Day-Jones A. C., Jones H. R. A., Murray D., Nickson E., Tamura M., Zhang Z., Lodieu N., Tinney C. G., Osorio M. R. Z., 2010a, *MNRAS*, 404, 1952  
 Burningham B., Pinfield D. J., Leggett S. K., Tamura M., Lucas P. W., Homeier D., Day-Jones A., Jones H. R. A., Clarke J. R. A., Ishii M., Kuzuhara M., Lodieu N., Zapatero Osorio M. R., Venemans B. P., Mortlock D. J., Bar-

- rado Y Navascués D., Martin E. L., Magazzù A., 2008, *MNRAS*, 391, 320
- Burningham B., Pinfield D. J., Leggett S. K., Tinney C. G., Liu M. C., Homeier D., West A. A., Day-Jones A., Huelamo N., Dupuy T. J., Zhang Z., Murray D. N., Lodieu N., Barrado Y Navascués D., Folkes S., Galvez-Ortiz M. C., Jones H. R. A., Lucas P. W., Calderon M. M., Tamura M., 2009, *MNRAS*, 395, 1237
- Burningham B., Pinfield D. J., Lucas P. W., Leggett S. K., Deacon N. R., Tamura M., Tinney C. G., Lodieu N., Zhang Z. H., Huelamo N., Jones H. R. A., Murray D. N., Mortlock D. J., Patel M., Navascues D. B. y., Zapatero Osorio M. R., Ishii M., Kuzuhara M., Smart R. L., 2010b, *ArXiv e-prints*
- Casali M., Adamson A., Alves de Oliveira C., Almaini O., Burch K., Chuter T., Elliot J., Folger M., Foucaud S., Hambly N., Hastie M., Henry D., Hirst P., Irwin M., Ives D., Lawrence A., Laidlaw K., Lee D., Lewis J., Lunney D., McLay S., Montgomery D., Pickup A., Read M., Rees N., Robson I., Sekiguchi K., Vick A., Warren S., Woodward B., 2007, *A&A*, 467, 777
- Cushing M. C., Marley M. S., Saumon D., Kelly B. C., Vacca W. D., Rayner J. T., Freedman R. S., Lodders K., Roellig T. L., 2008, *ApJ*, 678, 1372
- Day-Jones A. C., Pinfield D. J., Napiwotzki R., Burningham B., Jenkins J. S., Jones H. R. A., Folkes S. L., Weights D. J., Clarke J. R. A., 2008, *MNRAS*, 388, 838
- Day-Jones A. C., Pinfield D. J., Ruiz M. T., Beaumont H., Burningham B., Gallardo J., Gianninas A., Bergeron P., Napiwotzki R., Jenkins J. S., Zhang Z. H., Murray D., Catalan S., Gomes J., 2010, *ArXiv e-prints*
- Dupuy T. J., Liu M. C., Ireland M. J., 2009, *ApJ*, 699, 168
- Goldman B., Marsat S., Henning T., Clemens C., Greiner J., 2010, *MNRAS*, 405, 1140
- Hambly N. C., Collins R. S., Cross N. J. G., Mann R. G., Read M. A., Sutorius E. T. W., Bond I., Bryant J., Emerson J. P., Lawrence A., Rimoldini L., Stewart J. M., Williams P. M., Adamson A., Hirst P., Dye S., Warren S. J., 2008, *MNRAS*, 384, 637
- Hawley S. L., Gizis J. E., Reid N. I., 1997, *AJ*, 113, 1458
- Hodapp K. W., Jensen J. B., Irwin E. M., Yamada H., Chung R., Fletcher K., Robertson L., Hora J. L., Simons D. A., Mays W., Nolan R., Bec M., Merrill M., Fowler A. M., 2003, *PASP*, 115, 1388
- Irwin M. J., Lewis J., Hodgkin S., Bunclark P., Evans D., McMahon R., Emerson J. P., Stewart M., Beard S., 2004, in *Society of Photo-Optical Instrumentation Engineers (SPIE) Conference Series*, Vol. 5493, Society of Photo-Optical Instrumentation Engineers (SPIE) Conference Series, P. J. Quinn & A. Bridger, ed., pp. 411–422
- Johnson J. A., Apps K., 2009, *ApJ*, 699, 933
- King R. R., McCaughrean M. J., Homeier D., Allard F., Scholz R., Lodieu N., 2010, *A&A*, 510, A99+
- Kobayashi N., Tokunaga A. T., Terada H., Goto M., Weber M., Potter R., Onaka P. M., Ching G. K., Young T. T., Fletcher K., Neil D., Robertson L., Cook D., Imanishi M., Warren D. W., 2000, in *Presented at the Society of Photo-Optical Instrumentation Engineers (SPIE) Conference*, Vol. 4008, *Proc. SPIE Vol. 4008*, p. 1056–1066, Optical and IR Telescope Instrumentation and Detectors, Masanori Iye; Alan F. Moorwood; Eds., Iye M., Moorwood A. F., eds., pp. 1056–1066
- Lawrence A., Warren S. J., Almaini O., Edge A. C., Hambly N. C., Jameson R. F., Lucas P., Casali M., Adamson A., and thirteen co-authors, 2007, *MNRAS*, 379, 1599
- Leggett S. K., Burningham B., Saumon D., Marley M. S., Warren S. J., Smart R. L., Jones H. R. A., Lucas P. W., Pinfield D. J., Tamura M., 2010, *ApJ*, 710, 1627
- Littlefair S. P., Dhillon V. S., Marsh T. R., Gänsicke B. T., Baraffe I., Watson C. A., 2007, *MNRAS*, 381, 827
- Lodieu N., Pinfield D. J., Leggett S. K., Jameson R. F., Mortlock D. J., Warren S. J., Burningham B., Lucas P. W., Chiu K., Liu M. C., Venemans B. P., McMahon R. G., Allard F., Baraffe I., Y Navascués D. B., Carraro G., Casewell S. L., Chabrier G., Chappelle R. J., Clarke F., Day-Jones A. C., Deacon N. R., Dobbie P. D., Folkes S. L., Hambly N. C., Hewett P. C., Hodgkin S. T., Jones H. R. A., Kendall T. R., Magazzù A., Martín E. L., McCaughrean M. J., Nakajima T., Pavlenko Y., Tamura M., Tinney C. G., Zapatero Osorio M. R., 2007, *MNRAS*, 379, 1423
- McLean I. S., Smith E. C., Aliado T., Brims G., Kress E., Magnone E., Milburn J., Oldag A., Silvers T., Skulason G., Becklin E. E., Shuping R. Y., 2006, in *Society of Photo-Optical Instrumentation Engineers (SPIE) Conference Series*, Vol. 6269, Society of Photo-Optical Instrumentation Engineers (SPIE) Conference Series
- Morales J. C., Ribas I., Jordi C., 2008, *A&A*, 478, 507
- Nakajima T., Oppenheimer B. R., Kulkarni S. R., Golimowski D. A., Matthews K., Durrance S. T., 1995, *Nature*, 378, 463
- Nidever D. L., Marcy G. W., Butler R. P., Fischer D. A., Vogt S. S., 2002, *ApJS*, 141, 503
- Pinfield D. J., Burningham B., Tamura M., Leggett S. K., Lodieu N., Lucas P. W., Mortlock D. J., Warren S. J., Homeier D., Ishii M., Deacon N. R., McMahon R. G., Hewett P. C., Osori M. R. Z., Martin E. L., Jones H. R. A., Venemans B. P., Day-Jones A. C., Dobbie P. D., Folkes S. L., Dye S., Allard F., Baraffe I., Barrado Y Navascués D., Casewell S. L., Chiu K., Chabrier G., Clarke F., Hodgkin S. T., Magazzù A., McCaughrean M. J., Nakajima T., Pavlenko Y., Tinney C. G., 2008, *MNRAS*, 390, 304
- Pinfield D. J., Jones H. R. A., Lucas P. W., Kendall T. R., Folkes S. L., Day-Jones A. C., Chappelle R. J., Steele I. A., 2006, *MNRAS*, 368, 1281
- Saumon D., Marley M. S., 2008, *ApJ*, 689, 1327
- Saumon D., Marley M. S., Cushing M. C., Leggett S. K., Roellig T. L., Lodders K., Freedman R. S., 2006, *ApJ*, 647, 552
- Saumon D., Marley M. S., Leggett S. K., Geballe T. R., Stephens D., Golimowski D. A., Cushing M. C., Fan X., Rayner J. T., Lodders K., Freedman R. S., 2007, *ApJ*, 656, 1136
- Schlaufman K. C., Laughlin G., 2010, *A&A*, 519, A105+
- Scholz R., 2010, *ArXiv e-prints*
- Scholz R.-D., McCaughrean M. J., Lodieu N., Kuhlbrodt B., 2003, *A&A*, 398, L29
- Stassun K. G., Mathieu R. D., Valenti J. A., 2006, *Nature*, 440, 311
- Tokunaga A. T., Simons D. A., Vacca W. D., 2002, *PASP*, 114, 180
- Visscher C., Moses J. I., Saslow S. A., 2010, *Icarus*, 209, 602

West A. A., Hawley S. L., Bochanski J. J., Covey K. R.,  
Reid I. N., Dhital S., Hilton E. J., Masuda M., 2008, *AJ*,  
135, 785  
Yamamura I., Tsuji T., Tanabé T., 2010, *ApJ*, 722, 682  
Zhang Z. H., Pinfield D. J., Day-Jones A. C., Burningham  
B., Jones H. R. A., Yu S., Jenkins J. S., Han Z., Gálvez-  
Ortiz M. C., Gallardo J., García-Pérez A. E., Weights D.,  
Tinney C. G., Pokorny R. S., 2010, *MNRAS*, 404, 1817